Investigation of an Optimized Buckling-Resistant Structural Fuse Shape

Trai Nguyen[1], Javier Avecillas[1], Matthew Eatherton[2]

[1] Graduate Research Assistant, Department of Civil and Environmental Engineering, Virginia Tech, Blacksburg, USA.
[2] Associate Professor, Department of Civil and Environmental Engineering, Virginia Tech, Blacksburg, USA.

ABSTRACT

A number of seismic lateral force resisting systems depend on the ductile energy-dissipating behavior of steel plates deforming in shear (e.g. steel plate shear walls, link beam in eccentrically braced frames, steel coupling beams in hybrid coupled shear walls, the linked column system). However, these steel shear plates can be prone to undesirable limit states such as buckling at small shear force for steel plate shear walls or fracture at relatively small shear angle for eccentrically braced frame link beams. Recently, topology optimization has been used to develop several optimized structural fuse shapes using an objective function that was designed to discourage buckling and promote yielding in a square domain between a fixed edge and an opposing edge that is subjected to racking shear displacements. The resulting optimized topologies are shown to offer significant advantages in terms of buckling resistance, energy dissipation, and material efficiency.

This paper briefly describes how optimized structural fuse shapes were generated using a genetic algorithm based topology optimization procedure. The results of the topology optimization are unique pixelated shapes that can be difficult to adapt to different design settings. To make the topologies more practical and adaptable, one of the shapes is parameterized as a function of five design variables. Plastic mechanism analysis is then used to develop a generalized equation for shear strength. Finally, a parametric finite element study is conducted to evaluate the effect of varying two of the key parameters on strength, stiffness, out-of-plane buckling, accumulated plastic strain and energy dissipation.

Keywords: Structural Fuses, Plate Buckling, Topology Optimization, Plastic Analysis, Seismic Behavior.

INTRODUCTION

One approach to earthquake resistant structural design is to concentrate damage in replaceable structural fuses, thus limiting inelastic deformations in the rest of the structure. In some configurations, these structural fuses can be plates subjected to shear deformations. In particular, elements of lateral force resisting systems that could be replaced by a shear acting structural fuse include the link beam in eccentrically braced frames, the coupling beam in coupled shear walls, and the link element in the linked column system [1-3]. Shear acting structural fuses might consist of steel plates with a set of strategic cutouts that dissipate energy by converting global shear deformations into local yielding mechanisms. However, conventional ductile shear-acting elements of lateral force resisting systems as well as their shear-acting structural fuse counterparts can be prone to undesirable limit states such as buckling at small levels of shear deformations or fracture.

An example of a ductile shear-acting structural fuse shape is the butterfly-shaped link that was shown by Ma et al. [4] to have very ductile hysteretic behavior with large deformation capacity. Egorova et al. [5] studied the hysteretic behavior of ring-shaped structural fuses that were conceived specifically to prevent shear buckling. Deng et al. [6] used external stiffeners to help control the out-of-plane deformations and limit buckling. Topology optimization was used by Liu and Shimoda [7] for shear-acting structural fuses where the objective function was taken as the cumulative plastic strain, while Ghabraie et al. [8] used topology optimization to maximize the dissipated energy.

Recently a topology optimization study was conducted to minimize out-of-plane buckling of an unstiffened steel plate [9]. This paper starts with a brief summary of the topology optimization procedure along with some resulting shapes. However, it can be difficult to adapt the results of topology optimization to different design situations (i.e. building specific needs for strength, deformation capacity, or stiffness). To make the optimized structural fuse shape more usable for general seismic design, the shape is described by a set of five unique parameters and all other dimensions are assumed to be functions of these five design parameters. Then plastic mechanism analysis is used to derive a generalized equation for the shear strength of the parameterized shape. To evaluate the effect of the design parameters on the cyclic behavior of the structural fuse, two of the key design parameters are varied and their effect on strength, stiffness, out-of-plane buckling, accumulated plastic strain and energy dissipation are evaluated.

TOPOLOGY OPTIMIZATION OF STRUCTURAL FUSES

Optimization Setup

The goal of this topology optimization is to find a distribution of material that resists buckling while undergoing yielding. The domain is square (711mm x711mm or 28 in x 28 in) with thickness of t=12.7 mm (or t=0.5 in.), discretized into a 32x32 element mesh, as shown in Figure 1(a). This domain has a fixed edge and an opposing edge that is subjected to racking shear displacement. The goal of the topology optimization is to maximize the elastic shear buckling load, V_B, as compared to the inelastic shear yield load, V_Y, while also encouraging both V_B and V_Y to be as large as possible.
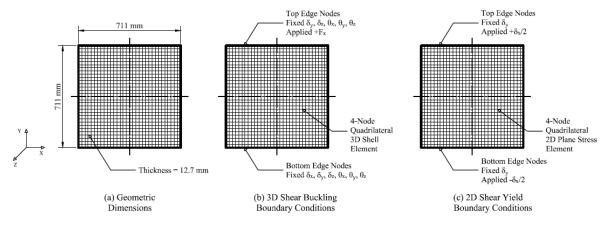

Figure 1. Domain and boundary conditions for finite element analyses

The elastic shear buckling load, V_B, is obtained from a three-dimensional linear eigenbuckling analysis considering the boundary conditions illustrated in Figure 1(b), and the shear yield load, V_Y, is obtained from a two-dimensional material-nonlinear FE analysis assuming the boundary conditions shown in Figure 1(c). The material properties used in the FE analyses correspond to ASTM A572 Grade 50 steel plate material with a Young's modulus of E=200,000 MPa and a Poisson's ratio of ν=0.3. The inelastic regime is modeled as linear kinematic hardening with yield strength of 345 MPa and a hardening slope equal to H=2,000 MPa. Finite element analyses are performed using Finite Element Analysis Program (FEAP), Taylor [10].

Based on the geometric dimensions and material properties described above and a target volume fraction of 40% of the full domain, the objective function used in the optimization procedure is given in Eq. 1. The numerator consists of a normalizing constant described in Avecillas [9] where f_Y=345 MPa, w=711 mm, and t=12.7 mm. The first term in the denominator encourages the optimized topology to have a ratio $V_Y/V_B=k$, (in this paper k=0.1 or k=0.2) where the value of k less than unity implies the structural fuse will experience some yielding before elastic buckling and low values of k, such as 0.1 or 0.2, imply that considerable yielding will occur before buckling occurs. The second term encourages the optimized topology to have the largest possible values of V_Y and V_B.

$$\underset{x}{\text{minimize}} : \mathrm{f}\left(x\right) = \frac{0.23 f_Y wt}{\exp\left[-50\left(\dfrac{V_Y}{V_B} - k\right)^2\right]\sqrt{V_Y^2 + V_B^2}} \tag{1}$$

The optimization procedure uses a genetic algorithm initialized with 100 topologies. These 100 topologies are divided into 95 randomly generated shapes, 1 topology representing the ring-shaped structural fuse [5], 3 variations of the butterfly-shaped fuse [4], and an X-shaped topology representing the maximum in-plane stiffness (see [9] for details). The algorithm is stopped after 400 generations and uses exponential ranking selection, a single-point crossover operation interchanging 50% of the topology's structure, and a 5% probability of mutation interchanging 10% of the topology volume. Given the loading conditions associated with a steel structural fuse, a doubly symmetric topology is assumed which is enforced by operating with only one quarter of the actual topology. Also, if a shape lacks a load path or has disconnected structural components, the topology is repaired according to the algorithm by Madeira et al. [11] only if the largest disconnected component has at least 90% of the target volume. Additional details on the topology optimization can be found in Avecillas [9].

Optimized Topologies

The evolution of the objective function associated with the best topology during the optimization algorithm is illustrated in Figure 2(a). For the ratio V_Y/V_B=0.2 (i.e. k=0.2 in Eq. 1), the final topology is presented in Figure 2(b). This optimized topology is associated with an objective function value equal to $f(x)$=0.757, corresponding to V_B=933 kN and V_Y=184 kN. Similarly, the optimized topology when V_Y/V_B=0.1 is shown in Figure 2(c), and it is associated with an objective function value equal to $f(x)$=0.835 corresponding to V_B=866 kN and V_Y=99.9 kN.

(a) Evolution of the Objective Function (b) Optimized Topology - V_Y/V_B=0.2 (c) Optimized Topology - V_Y/V_B=0.1
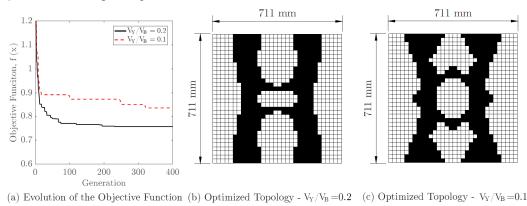
Figure 2: Evolution of the objective function and optimized topologies for a target volume of 40%

BEHAVIOR OF OPTIMIZED TOPOLOGIES

To get the hysteretic response of the optimized topologies, finite element models are created using ABAQUS [12]. First, each optimized topology is converted into a smooth version of its pixelated predecessor, as illustrated in Figure 3(a) and 3(b). Then, the topologies are modeled using 4-node full integration shell elements with an approximate mesh size of 12 mm. The material is modeled as elastic isotropic with a linear kinematic hardening rule as described in the previous section. In addition to consideration of nonlinear geometric behavior, initial imperfections are taken as the first buckling mode shape scaled by a factor of H/250. The cyclic displacement protocol is an adaptation of the qualifying cyclic test of link-to-column moment connections in eccentrically braced frames [13]. Finally, the cyclic responses of both optimized topologies are presented in Figure 3(c). It is observed that the optimized structural fuses exhibit full hysteretic behavior without the stiffness or strength degradation typically associated with buckling up to large drift angles. For V_Y/V_B=0.2, the strength degradation associated with buckling occurs at approximately 4% drift angle, and for V_Y/V_B=0.1, no strength degradation or buckling is observed up to 9% drift angle.

(a) Smooth shape and FE model - V_Y/V_B = 0.2 (b) Smooth shape and FE model - V_Y/V_B = 0.1 (c) Cyclic behavior
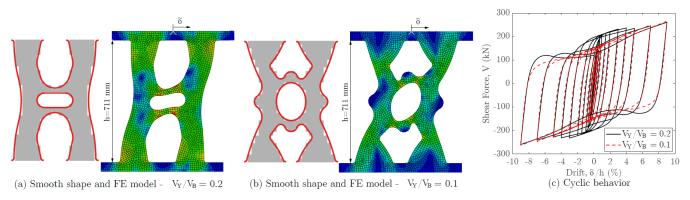
Figure 3: Cyclic behavior of both optimized topologies

PARAMETERIZATION

Optimized topologies are hard to implement in real structures, because they represent one geometry with a set shear strength and stiffness. For a topology to be useful in design, the strength should be predictable and adjustable while the geometry should be adaptable to different configurations and sizes. Therefore, a two-part interpretation of the optimized shape is conducted. First, smooth curves are fit to the pixilated shape as shown in Figure 4(a) and second the geometry is simplified into a function of a small number of geometrical parameters. For instance, the topology shown in Figure 4(b) has been smoothed and simplified as a function of five design variables and the rest of the geometry is dependent on these variables.

The design parameters are the tie width W_T, leg width W_L, radius at tie R_1, structural fuse height, L, and plate thickness, t. The relationship between the dependent parts of the geometry and the design parameters is taken from the optimized topology and assumed to be linearly related to the design parameters, W_L or L. For the topology to be reasonable, there need to be limits on the design parameters. It was determined that the following limits are required to make the parameterized topology geometrically possible: $L/W_T > 4.35$ and $R_1/W_L > 0.5$.

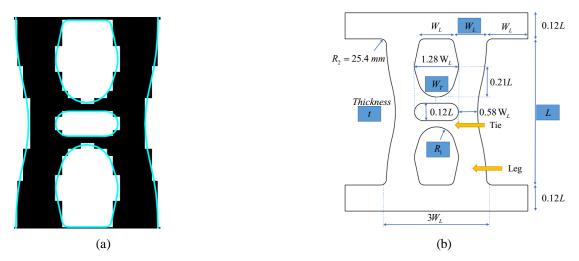(a)   (b)

Figure 4. (a) Smoothed curves over pixelated topology, (b) Parameters

PLASTIC ANALYSIS

For structural analysis purposes, the optimized shape is idealized by centerline elements as shown in Figure 5(a). Two key variables for the plastic analysis are the width of the leg plastic hinge, W_{LP}, and the width of the tie, W_{TP}, which are shown on Figure 5(a).

(a)   (b)   (c)
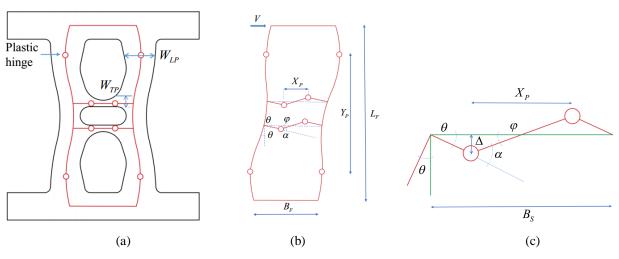
Figure 5. (a) Un-deformed shape, (b) Deformed shape, (c) Tie configuration

The distance between the plastic hinges in the tie, X_P, can be determined analytically. The plastic moment capacity, M_P, of the tie along its length at any location, x, is given by Eq. (2) with coordinate system shown in Figure 6(a). The moment demand, M_d, is linearly varying and given by Eq. (3). Setting the moment capacity equal to the moment demand, solving for the shear force V, and then setting the derivative equal to zero, finds the value of x that minimizes the shear strength, V. Two times this value of x gives the distance, X_p, in Eq. (4). A plot of the plastic moment strength and moment demand (See Figure 6(b)) demonstrates that the moment demand, M_d, first reaches the plastic moment strength, M_p, at the locations described by X_p in Eq. (4).

$$M_p(x) = f_y \frac{t}{4} W^2(x) = \frac{tf_y}{4}(W_T + R_1 - \sqrt{R_1^2 - x^2})^2 \qquad (2)$$

$$M_d(x) = Vx \qquad (3)$$

$$X_P = \sqrt{2}\sqrt{(W_T + R_1)\sqrt{(W_T + R_1)^2 + 8R_1^2} - (W_T + R_1)^2 - 2R_1^2} \qquad (4)$$
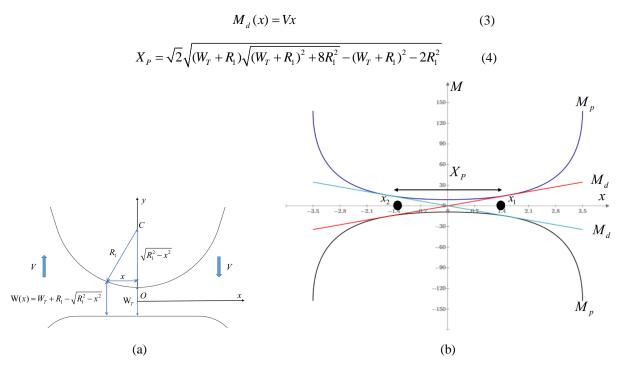

(a)

(b)

Figure 6. (a) Local coordinate system, (b) Locations of plastic hinges

The plastic mechanism is shown in Figure 5(b) and virtual work is used to find the shear strength. The external work is given by the left side of Eq. (5) while the internal work is given by the right side of Eq. (5). After substituting the equations in Eq. (6) for plastic moment strength for the leg, M_L, and the tie, M_T, and defining the relationship between the tie angle, α, and the leg angle, θ, (see Figure 5(c)), the equation of shear strength can be obtained as given in Eq. (7). Based on observations about the locations of plastic strain concentrations in the finite element model shown in Figure 3(a), Eq. (7) can be converted to a function of the five design parameters by using the following approximations: the location of the leg plastic hinge is approximated as $Y_P \approx L - 0.5W_L$, and the width of the leg and tie at the plastic hinges are approximated as, $W_{LP} \approx 0.85W_L$ and $W_{LP} \approx 1.25\ W_T$, respectively. It is noted, that these approximations are not valid if the design parameters vary too much from the optimized topology. If a more accurate solution is desired, the width of the tie at the plastic hinge can be found based on Eq. (4) and Figure 6(a) and a similar methodology could be used to obtain the location and width of the leg plastic hinge. Substituting the approximate dimensions results in the shear strength equation given in Eq. (8).

$$V(Y_P, \theta) = 4(M_L\theta + M_T\alpha) \qquad (5)$$

$$M_L = f_y\frac{tW_{LP}^2}{4} \qquad M_T = f_y\frac{tW_{TP}^2}{4} \qquad \alpha = \frac{B_S}{X_P}\theta \qquad (6)$$

$$V = \frac{tf_y}{Y_P}(W_{LP}^2 + \frac{B_S W_{TP}^2}{X_P}) \qquad (7)$$

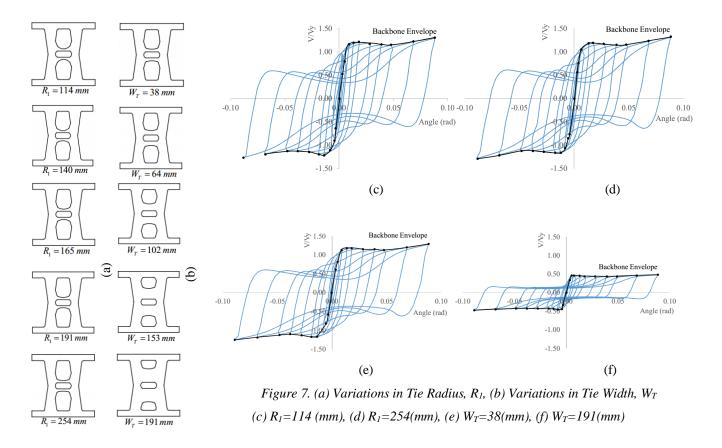$$V \approx \frac{tf_y}{L - 0.5W_L}[(0.85W_L)^2 + \frac{B_S}{X_P}(1.25W_T)^2] \qquad (8)$$

PARAMETRIC STUDY

The parametric study has several purposes including 1) evaluating whether changing the design variables can decrease the equivalent plastic strain and thus reduce the potential for fracture, 2) determining whether changing the design variables affects the observed plastic mechanism and therefore the ability of Eq. (8) to predict shear strength, and 3) investigating whether shapes with different values of the design variables have as much buckling resistance as the original optimized topology. The first set of topologies shown in Figure 7(a) have constant values of W_T=30 mm, W_L=118 mm, L=711 mm, and t=13 mm, while the tie radius, R_1, is varied to have values of 114 mm, 140 mm, 165 mm, 191 mm and 254 mm. The second set of topologies is shown in Figure 7(b) which all have constant values of R_1=254 mm, W_L=118 mm, L=711 mm, and t=13

mm, while the tie width, W_T, is varied to be 38 mm, 64 mm, 102 mm, 153 mm, 191 mm. For reference, the parameters for the optimized topology are: R_1=89 mm, W_T=30 mm, W_L=118 mm, L=711 mm, and t=13 mm.

The computational models are similar to those described previously for the original optimized topologies. Initial imperfections are applied in the shape of the first elastic buckling mode with maximum out-of-plane displacement value of L/250. Computational parametric study is performed using LS-DYNA [14] with the eccentrically braced frame displacement protocol [13]. Load-displacement curves are shown in Figure 7(c) through 7(f) for four of the models, R$_1$=114 mm, R$_1$=254 mm, W$_T$=38 mm, and W$_T$=191 mm. It is observed that all four of these geometries have substantially more pinching than the optimized topology and all of these models experienced out-of-plane buckling. This suggests that it may not be easy to vary the geometry of the shape and retain the advantageous buckling resistance. From the differences between the shear angle at which pinching begins and the severity of the pinching, it is seen that the tie radius, R_1, does not have much effect on hysteretic shape, while the tie width, W_T, has a substantial effect on pinching and thus buckling. Comparing Figure 7(e) with 7(f), increasing the tie width from 38 mm to 191 mm greatly reduces the shear angle at which buckling starts changing the load-deformation behavior.

Figure 7. (a) Variations in Tie Radius, R_1, (b) Variations in Tie Width, W_T
(c) R_1=114 (mm), (d) R_1=254(mm), (e) W_T=38(mm), (f) W_T=191(mm)

Strength and stiffness

Both computational strength from the finite element models and the predicted values using Eq. (8) are shown in Figure 8. By increasing radius, R_1, both shear strength and stiffness reduce gradually. Numerically, by increasing radius by 123% (going from R_1=114 mm to R_1=254 mm), the strength and stiffness reduce by 5.5% and 24%, respectively. In one way, the reduction in strength and stiffness can be explained by a decrease of volume fraction as the radius increases. Another way to view the result is that reducing the average width of the tie decreases the degree of coupling between the legs. Conversely, as the tie width gets larger, the volume fraction increases and the coupling between the legs gets stronger, thus increasing the strength and stiffness. An increase of tie width by 400% (W_T=38 mm to W_T=191 mm) results in the increase of strength and stiffness by approximately 423% and 256%, respectively. Figure 8 and Figure 9 show that both strength and stiffness of structural fuse are more sensitive to tie width than tie radius. It is noted that the predicted strength from Eq. (8) matches well the computational strength (4% errors) for the range of tie radius studied (see Fig. 8a), but as the tie width gets bigger, this equation cannot accurately predict shear strength due to the change of plastic mechanism (i.e. the plastic mechanism in Figure 5b is no longer valid).
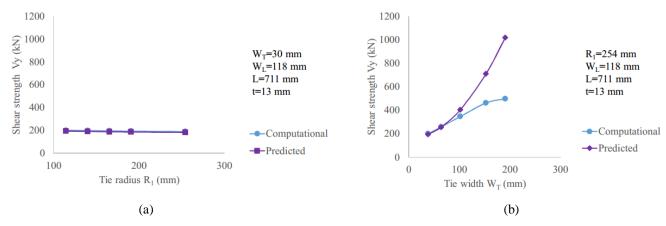
Figure 8. Strength with (a) Variations in R_1, (b) Variations in W_T
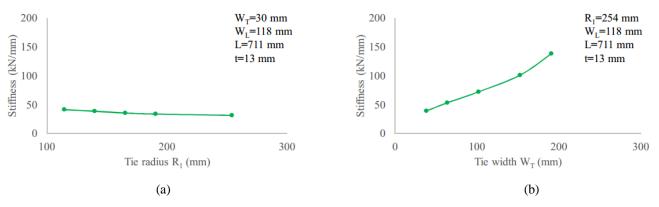

Figure 9. Stiffness with (a) Variations in R_1, (b) Variations in W_T

Buckling

It can be seen that increasing the tie radius by 123% (R_1=114 mm vs. R_1=254 mm) results in an increase of out-of-plane displacement by just 8.5% while increasing tie width by 400% (W_T=38 mm vs. W_T=191 mm) results in an increase of 51%. This suggests that tie width is more important than radius in buckling-resistant capacity of structural fuse.
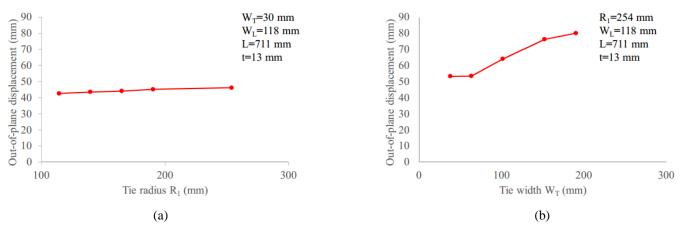

Figure 10. Out-of-plane displacement with: (a) Variations in R_1, (b) Variations in W_T

Equivalent plastic strain

Figure 11 indicates that reducing tie radius results in the reduction of equivalent plastic strain while an increase in tie width leads to the significant increase in equivalent plastic strain. This suggests that increasing tie radius and reducing tie width simultaneously may mitigate the potential for fracture due to excessive equivalent plastic strain. Separately, it is noted that as

7

the tie width gets bigger, the plastic mechanism is expected to change and thus locations of the largest equivalent plastic strains and potential fracture locations will change.
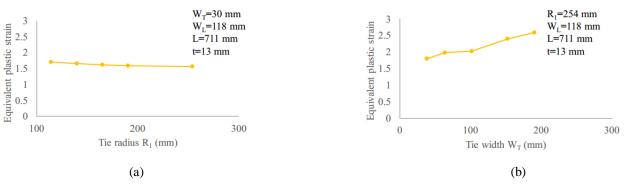

(a)   (b)

Figure 11. Equivalent plastic strain with: (a) Variations in R_1, (b) Variations in W_T

CONCLUSIONS

The parameterization of optimized structural fuse topologies is an important step in bridging the gap between topology optimization and practical design. Plastic analysis was used to propose two equations, one to predict the locations of plastic hinges, and the second to determine shear strength based on the parameterized geometrical dimensions. Results from predicted equations match well with the computational values as long as the geometry isn't varied so much that the plastic mechanism changes. The results from a small parametric study indicate that strength, stiffness, buckling and energy dissipation of structural fuse are more sensitive to tie width than to tie radius. It is suggested that increasing tie radius and decreasing tie width at the same time is a promising approach to mitigate the potential for fracture.

ACKNOWLEDGMENTS

REFERENCES

[1]   Borello, D. and Fahnestock, L. (2012). Seismic design and analysis of steel plate shear walls with coupling. Journal of Structural Engineering

[2]   Popov, Egor & Engelhardt, Michael. (1988). Seismic eccentrically braced frames. Journal of Constructional Steel Research. 10. 321-354. 10.1016/0143-974X(88)90034-X.

[3]   Malakoutian, M. , Berman, J. W. and Dusicka, P. (2013), Seismic response evaluation of the linked column frame system. Earthquake Engng Struct. Dyn., 42: 795-814. doi:10.1002/eqe.2245

[4]   Ma, X., Borchers, E., Pena, A., Krawinkler, H. and Deierlein, G. (2010). "Design and behavior of steel shear plates with openings as energy-dissipating fuses." John A. Blume Earthquake Engineering Center Technical Report, (173).

[5]   Egorova, N., Eatherton, M. R. and Maurya, A. (2014). "Experimental study of ring-shaped steel plate shear walls." Journal of Constructional Steel Research, 103, 179-189.

[6]   Deng, K., Pan, P., Li, W. and Xue, Y. (2015). "Development of a buckling restrained shear panel damper." Journal of Constructional Steel Research, 106(1), 311-321.

[7]   Liu, Y. and Shimoda, M. (2013). "Shape optimization of shear panel damper for improving the deformation ability under cyclic loading." Structural and Multidisciplinary Optimization, 48(2), 427-435.

[8]   Ghabraie, K., Chan, R., Huang, X. and Xie, Y. M. (2010). "Shape optimization of metallic yielding devices for passive mitigation of seismic energy." Engineering Structures, 32(8), 2258-2267.

[9]   Avecillas, J. (2018). "Topology optimization of steel shear fuses to resist buckling". Master's thesis. Virginia Polytechnic Institute and State University.

[10] Taylor, R. L. (2013). "Feap version 8.4 user manual." University of California at Berkeley.

[11] Madeira, J. A., Rodrigues, H. and Pina, H. (2006). "Multi-objective topology optimization of structures using genetic algorithms with chromosome repairing." Structural and Multidisciplinary Optimization, 32(1), 31-39.

[12] ABAQUS - 2002-2018 Dassault Systèmes - https://www.3ds.com/products-services/simulia/products/abaqus/

[13] AISC (2016). "Seismic provision for structural steel buildings." ANSI/AISC 341-16.

[14] LS-DYNA. 2011-2018 LSTC. http://www.lstc.com/